Bifurcations of the global stable set of a planar endomorphism near a cusp singularity

C.A. Hobbs
School of Technology,
Oxford Brookes University
Wheatley Campus, Oxford, OX33 1HX, UK

H.M. Osinga
Bristol Centre for Applied Nonlinear Mathematics,
Department of Engineering Mathematics,
University of Bristol, Queen's Building, Bristol BS8 1TR, UK

Keywords: stable manifold, stable set, backward invariant, cusp singularity, critical locus, unfolding

Abstract

The dynamics of a system defined by an endomorphism is essentially different from that of a system defined by a diffeomorphism due to interaction of invariant objects with the so-called critical locus. A planar endomorphism typically folds the phase space along curves J_0 where the Jacobian of the map is singular. The critical locus, denoted J_1, is the image of J_0. It is often only piecewise smooth due to the presence of isolated cusp points that are persistent under perturbation. We investigate what happens when the stable set W^s of a fixed point or periodic orbit interacts with J_1 near such a cusp point C_1. Our approach is in the spirit of bifurcation theory, and we classify the different unfoldings of the codimension-two singularity where the curve W^s is tangent to J_1 exactly at C_1. The analysis uses a local normal-form setup that identifies the possible local phase portraits. These local phase portraits give rise to different global manifestations of the behaviour as organised by five different global bifurcation diagrams.

1 Introduction

When time-varying processes are modelled by discrete dynamical systems, one often finds that this gives rise to noninvertible maps. The classic example is an adaptive control system with a time delay [Adomaitis & Kevrekidis, 1991, Frouzakis *et al.*, 1992]. If the sampling time for constructing the feedback control is too large, the resulting system is not invertible. Another example is the so-called overcompensatory Leslie population model for age-structured populations in ecology [Wikan & Mjølhus, 1996, Ugarcovici & Weiss, 2004].

Here, the assumption that fertility rates decay exponentially with population size introduces noninvertibility into the model.

The main focus of interest in noninvertible systems has been on the structure of basins of attraction, where the phase space of the system in question is usually two dimensional. The noninvertibility of the map can give rise to an unusually complex basin and there are many case studies reporting on different phenomena; recent examples are [Agliari, 2000], [Agliari *et al.*, 2003], [Bischi *et al.*, 2006], [England *et al.*, 2004], [England *et al.*, 2005], and [López-Ruiz & Fournier-Prunaret, 2003]. Indeed, smooth noninvertible maps (endomorphisms) on the plane typically fold the phase space to give regions that correspond to different numbers of preimages. The locus where the number of preimages changes is called the critical locus. The reported phenomena correspond to global bifurcations of the basin boundary as it interacts with the critical locus.

The setup for this paper is very similar to [Krauskopf *et al.*, 2007], namely, we consider a family of endomorphisms of the plane

$$\begin{array}{rccc} f & : & \mathbb{R}^2 \times \mathbb{R}^m & \to & \mathbb{R}^2 \\ & & (\boldsymbol{x}, \lambda) & \mapsto & f(\boldsymbol{x}, \lambda), \end{array}$$

with f a smooth function depending on an m-dimensional parameter $\lambda \in \mathbb{R}^m$. If f is not a diffeomorphism then the Jacobian Df of f has a nonzero kernel and we define the *singular locus*

$$J_0 := \ker(Df) = \{\boldsymbol{x} \in \mathbb{R}^2 \mid Df(\boldsymbol{x}) \text{ is singular}\}. \tag{1}$$

The image $J_1 := f(J_0)$, called the *critical locus*, divides the phase plane $\mathbb{R}^2$ into regions where the number of preimages is constant. Generically, J_0 is a smooth curve along which f folds the phase plane. The image J_1, however, may contain (isolated) cusp points, so that J_1 is generically only piecewise smooth. We are interested in how the dynamics are organised in a parameter-dependent way when a backward invariant object interacts with J_1 in the vicinity of a cusp point C_1. An object W is called backward invariant if all preimages of W are contained in W.

We are particularly interested in how a *stable set* associated with a fixed point or periodic orbit interacts with J_1, because such stable sets typically form the boundaries of basins of attraction. Indeed, the phenomena reported in the various case studies correspond to global bifurcations of a stable set that involve interactions with J_1. The stable set $W^s(\boldsymbol{x}_0)$, of a saddle fixed point $\boldsymbol{x}_0 = f(\boldsymbol{x}_0)$ is defined as the set of points that converge to $\boldsymbol{x}_0$ under forward iteration of f, that is,

$$W^s(\boldsymbol{x}_0) = \{\boldsymbol{x} \in \mathbb{R}^2 \mid f^n(\boldsymbol{x}) \to \boldsymbol{x}_0 \text{ as } n \to \infty\}. \tag{2}$$

If f is a diffeomorphism, then the Stable Manifold Theorem [Palis & de Melo, 1982] ensures the existence of $W^s(\boldsymbol{x}_0)$ as a smooth immersed manifold, provided $\boldsymbol{x}_0$ is hyperbolic, i.e., none of the eigenvalues of the Jacobian $Df(\boldsymbol{x}_0)$ are on the unit circle. Furthermore, $W^s(\boldsymbol{x}_0)$ has the same dimension as the number of stable eigenvalues and is tangent at $\boldsymbol{x}_0$ to the plane spanned by the corresponding eigenvectors.

If f is an endomorphism then $\boldsymbol{x}_0$ is generically hyperbolic and $\boldsymbol{x}_0 \notin J_0$. Hence, locally near $\boldsymbol{x}_0$ we can define a unique inverse of f such that the Stable Manifold Theorem applies

and $W^s(\boldsymbol{x}_0)$ is a manifold at least locally near $\boldsymbol{x}_0$. However, globally $W^s(\boldsymbol{x}_0)$ may consist of several disjoint (immersed) manifolds that arise from the multiple preimages. Therefore, we speak of $W^s(\boldsymbol{x}_0)$ as the *stable set*. In the context of planar endomorphisms, $W^s(\boldsymbol{x}_0)$ is typically a set of one-dimensional smooth curves. Note that $W^s(\boldsymbol{x}_0)$ is backward invariant because it consists of all preimages of the *primary manifold*, i.e., the manifold that contains $\boldsymbol{x}_0$; the primary manifold is only forward invariant and all points on $W^s(\boldsymbol{x}_0)$ eventually map to the primary manifold.

As reported in [England *et al.*, 2005], from the point of view of bifurcation theory and singularity theory there are generically only two global bifurcations of codimension one. As a parameter is varied, part of the (one-dimensional) stable set either protrudes from a region with k preimages into a region with $k+2$ preimages, leading to a disjoint closed curve, or a segment that lies in a region with k preimages retracts so that it lies entirely in a region with $k+2$ preimages, which causes a reorganisation of connected components. The former bifurcation is called *outer-fold* and the latter *inner-fold* bifurcation; examples of phase portraits before and after these bifurcations are shown in the right column of Fig. 3, panels 1 and 2, and panels 4 and 3, respectively. Both bifurcations are tangencies with J_1 that change the geometry of the stable set locally near J_0. The different global manifestations of these bifurcations account for the different phenomena that have been observed in the literature; see [England *et al.*, 2005, England *et al.*, 2004] for details.

In the vicinity of a cusp point C_1 on J_1, the inner- and outer-fold bifurcations can happen in close succession. Furthermore, $W^s(\boldsymbol{x}_0)$ may pass through C_1 under parameter variation, which gives rise to another global bifurcation that alters the relative location of $W^s(\boldsymbol{x}_0)$. We call this the *cusp-transition* bifurcation. If we allow two parameters to vary, then it is generically possible for $W^s(\boldsymbol{x}_0)$ to undergo a cusp-transition bifurcation at C_1 on J_1 in such a way that $W^s(\boldsymbol{x}_0)$ is also tangent to J_1 at C_1. We call this codimension-two bifurcation point the *fold-cusp* bifurcation. The question is now what the generic two-parameter bifurcation diagram will look like, that is: what is the *unfolding* of the fold-cusp bifurcation? We take an approach that is similar to the analysis in [Krauskopf *et al.*, 2007] of the cusp-cusp bifurcation. The cusp-cusp bifurcation is organised by the interaction of an unstable manifold with J_0, which has a major effect on the relative location of the unstable manifold near J_1. In contrast, the unfolding of the fold-cusp bifurcation is organised by the interaction of $W^s(\boldsymbol{x}_0)$ near J_1 and it mainly affects the relative location of the stable set near J_0.

This paper is organised as follows. In the next section we describe the precise setup of the bifurcation analysis and explain the normal-form approach. Section 3 presents the codimension-one bifurcations of a parabola, which is assumed to be part of a stable set, as it interacts with the critical locus. In the normal form we can locate the codimension-one bifurcations analytically in a two-parameter setting, albeit in an implicit sense. The relative position of the codimension-one bifurcation curves leads to five topologically different two-parameter bifurcation diagrams. These two-parameter unfoldings are shown in Sec. 4 along with the associated global phase portraits. The transitions between the different unfoldings are organised by global bifurcations, either at infinity or outside a neighbourhood of the fold-cusp point. In Sec. 5 we use a notion of local topological equivalence to explain how the bifurcation diagram locally near the fold-cusp point leads to a further classification of global manifestations, both of the bifurcation diagrams and the associated global phase portraits. We end with a discussion and an outlook in Sec. 6.

2 Normal form setting of the fold-cusp bifurcation

As mentioned in the introduction, we are interested in the generic two-parameter unfolding of the codimension-two fold-cusp bifurcation where a backward invariant curve W is tangent to J_1 exactly at a cusp point C_1. To this end, we define a normal form that applies only in local neighbourhoods V of J_1 and U of J_0 around C_1 and its unique preimage $C_0 \in J_0$, respectively. As was done in [Krauskopf *et al.*, 2007], we assume that the local action of the map can be described by the normal form of a generic smooth planar map with a cusp point. We use the version that is embedded in three dimensions (rather than four) and define the normal form as

$$F : (x, y) \mapsto (z, y) = (-x^3 - 3xy, y), \tag{3}$$

where we made a convenient choice for the quadratic and cubic coefficients. We may think of the coordinates (x, y) and (z, y) as local coordinate systems defining the neighbourhoods U and V of the phase plane, respectively.

The Jacobian matrix of (3)

$$DF(x, y) = \begin{pmatrix} -3x^2 - 3y & -3x \\ 0 & 1 \end{pmatrix}$$

is singular along the critical curve

$$J_0 := \{y = -x^2\}, \tag{4}$$

and the image of J_0 is the standard cusp

$$J_1 := \left\{ z = \pm 2 \left(\sqrt{(-y)} \right)^3 \;\middle|\; y \leq 0 \right\}. \tag{5}$$

We note that the first and second derivatives of J_1 are

$$\frac{dz}{dy} = \mp 3\sqrt{-y} \qquad \text{and} \tag{6}$$

$$\frac{d^2z}{dy^2} = \pm \frac{3}{2\sqrt{-y}}, \tag{7}$$

respectively. Equation (3) defines a noninvertible dynamical system of type $Z_1 < Z_3$, which means that J_1 separates the phase plane into regions with one and three preimages. In this normal form the cusp point C_1 is the origin in the (z, y)-plane that uniquely maps backward to the origin in the (x, y)-plane. The cusp curve J_1 has two preimages, namely, J_0 and

$$\widehat{J_0} := \{y = -\tfrac{1}{4}x^2\}, \tag{8}$$

that coincide at the origin. The bifurcation analysis described here also applies in general to maps with local $Z_k < Z_{k+2}$ behaviour, $k \geq 1$, near C_1. Indeed, locally we can identify the three inverses that are involved in creating the cusp on J_1. The additional preimages act trivially in the unfolding.

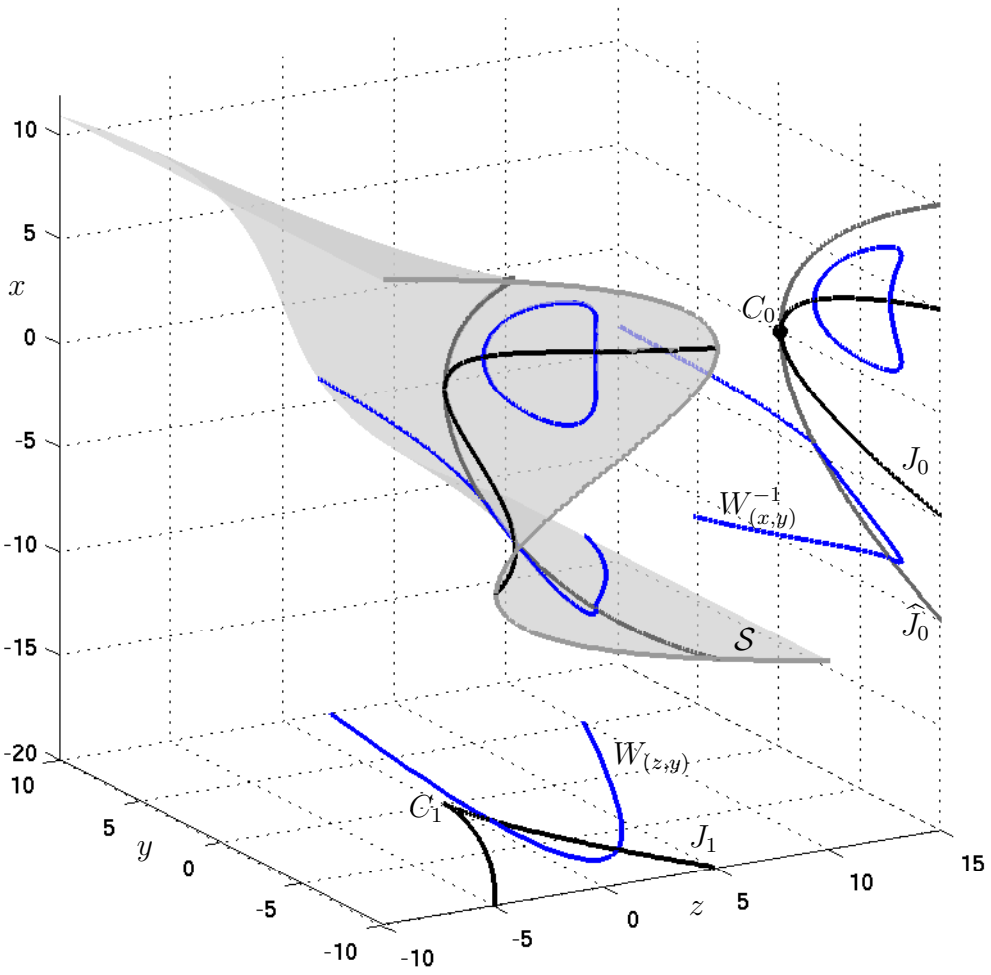

Figure 1: *The three-dimensional embedding of the normal-form map (3) shows how the action of the map can be interpreted as projections via a cusp surface $\mathcal{S}$. The preimages of a parabola $W_{(z,y)}$ in the (z,y)-plane are found by considering the lift of $W_{(z,y)}$ to $\mathcal{S}$, including all sheets. The projection onto the (x,y)-plane gives the set $W^{-1}_{(x,y)}$ of preimages. The example is topologically equivalent to phase portrait 2, shown in Fig. 3.*

Figure 1 illustrates how the normal-form map can be interpreted as a projection via the standard cusp surface $\mathcal{S} := \{z = -x^3 - 3xy\}$. A parabola is shown (labelled $W_{(z,y)}$) intersecting J_1 in the (z,y)-plane. This curve is lifted onto $\mathcal{S}$ creating several copies where $\mathcal{S}$ covers the (z,y)-plane more than once. The projection of each curve segment onto the (x,y)-plane gives the set $W^{-1}_{(x,y)}$ of preimages of $W_{(z,y)}$.

Generically, if two curves are tangent the tangency is quadratic. Hence, locally near the cusp point C_1 the interaction of a curve W with J_1 is quadratic. That is, W is locally a parabola that is part of a backward invariant set. To simplify the analysis, let us first assume that a *global* parabola W is part of a backward invariant set; in Sec. 5 we explain

how these global results are used to draw conclusions about the local behaviour. In the local (z, y)-coordinates the parabola W can be parametrised by $t \in \mathbb{R}$ as follows:

$$\begin{aligned} W_{(z,y)}(\theta, \gamma, a, b) \;&:=\; \begin{pmatrix} z \\ y \end{pmatrix} = R(\theta) \begin{pmatrix} \gamma t^2 \\ t \end{pmatrix} + \begin{pmatrix} a \\ b \end{pmatrix}, \\ &\text{where } R(\theta) = \begin{pmatrix} \cos\theta & -\sin\theta \\ \sin\theta & \cos\theta \end{pmatrix}. \end{aligned} \tag{9}$$

The angle θ controls the tilt of the parabola with respect to J_1 and $\gamma \neq 0$ controls the 'steepness' of the parabola. The vector $(a, b)^T$ translates the parabola in the phase plane. We think of θ and γ as higher-order coefficients and take a and b as the two unfolding parameters. Note that every segment of $W_{(z,y)}(\theta, \gamma, a, b)$ that lies above J_1 has a unique preimage, while every segment of the curve below J_1 will have three preimages that are not necessarily connected; see the example in Fig. 1. We let $W^{-1}_{(x,y)}$ denote the set of preimages of $W_{(z,y)}$, that is, $F(W^{-1}_{(x,y)}) = W_{(z,y)}$.

Our goal is to find all topologically different phase portraits that can arise by varying the parameters a and b in dependence on the higher-order coefficients θ and γ. Let us first explain precisely what we mean when two phase portraits are topologically different by giving our definition of topological equivalence.

Definition 2.1 (Topological equivalence with respect to J_1) *Two parabolic curves are topologically equivalent if the following holds:*

1. *Both parabolas asymptote to infinity in the region Z_1 above J_1, or both asymptote to infinity in the region Z_3 below J_1.*
2. *The number of intersection points with J_1 is the same.*
3. *The order in which these intersection points lie on J_1 relative to the cusp point C_1 is the same.*

With our notion of topological equivalence, we can make restrictions on the parameters without loss of generality. In particular, for given θ and $0 < \gamma_1 < \gamma_2$ or $\gamma_2 < \gamma_1 < 0$, we can find smooth functions a_2 and b_2 of parameters $a_1, b_1 \in \mathbb{R}$, such that the two curves $W_{(z,y)}(\theta, \gamma_1, a_1, b_1)$ and $W_{(z,y)}(\theta, \gamma_2, a_2, b_2)$ are topologically equivalent. Furthermore,

$$W_{(z,y)}(\theta, -\gamma, a, b) \equiv W_{(z,y)}(\theta + \pi, \gamma, a, b).$$

Hence, we may fix a value of $\gamma > 0$ (in Sec. 4 we use $\gamma = 1$). We also note that J_1 and J_0 are both symmetric about the respective vertical axes in the normal-form coordinates. Therefore, it suffices to restrict the angle to $-\frac{\pi}{2} \leq \theta \leq \frac{\pi}{2}$. In fact, the cases $\theta = \pm\frac{\pi}{2}$ are special, because $W_{(z,y)}(\pm\frac{\pi}{2}, \gamma, a, b)$ can never be tangent to J_1 at the cusp point for any finite value of a and b.

If we assume that θ and $\gamma > 0$ are fixed, then it is not possible to change the asymptotic direction of $W_{(z,y)}(\theta, \gamma, a, b)$, that is, we can always find $t_1, t_2 \in \mathbb{R}$ such that the two segments of $W_{(z,y)}(\theta, \gamma, a, b)$ with $t < t_1$ and $t > t_2$ in (9) lie entirely above or entirely below J_1. Therefore, the only way to create a topologically different phase portrait by varying a or b is to change the number of intersections between $W_{(z,y)}(\theta, \gamma, a, b)$ and J_1. In the next section we discuss all possible generic cases.

3 Codimension-one bifurcations

The global phase portrait of a parabola $W_{(z,y)}(\theta, \gamma, a, b)$ in the vicinity of a cusp point C_1 on J_1 is essentially determined by θ (we assume $\gamma > 0$ is fixed) and the intersections with J_1. Bezout's Theorem (see, for example, [Cox *et al.*, 1997]) implies that $W_{(z,y)}(\theta, \gamma, a, b)$ and J_1 have at most six intersection points. These are the roots of the degree-six curve in t given by equating (5) and (9):

$$(\gamma t^2 \cos\theta - t \sin\theta + a)^2 + 4(\gamma t^2 \sin\theta + t \cos\theta + b)^3 = 0. \tag{10}$$

Since a tangency of $W_{(z,y)}(\theta, \gamma, a, b)$ with J_1 is not generic, we expect that a typical parabola will have 0, 2, 4, or 6 intersections with J_1.

If we assume that θ and γ are fixed then there are three codimension-one bifurcations that change the number of intersections between a curve $W = W_{(z,y)}(\theta, \gamma, a, b)$ and J_1:

- At a *cusp-transition* bifurcation W passes through the cusp point C_1 on J_1.
- At an *inner-fold* bifurcation W is tangent to J_1 in such a way that locally near the tangency point W has three preimages.
- At an *outer-fold* bifurcation W is tangent to J_1 in such a way that locally near the tangency point W has a unique preimage.

All three bifurcations typically cause a change of two in the number of intersections. For the inner- and outer-fold bifurcations these two intersections lie at the same side of C_1, whereas for the cusp-transition bifurcation they lie on either side of C_1. Note that it is not typical to have an intersection move from one side of C_1 to the other: the cusp-transition bifurcation creates (or annihilates) two intersection points, except when W passes through C_1 exactly tangent at J_1, that is, when (a, b) is chosen at the fold-cusp point.

In the following sections we find an explicit formula for the fold-cusp bifurcation point and derive the codimension-one bifurcation curves analytically.

3.1 The codimension-two fold-cusp bifurcation

The fold-cusp bifurcation point, denoted FC is defined as the moment where a parabola W passes through the cusp point C_1 such that W is tangent to J_1 at C_1. For $W = W_{(z,y)}(\theta, \gamma, a, b)$ we have

$$\frac{dz}{dy} = \frac{2\gamma t \cos\theta - \sin\theta}{2\gamma t \sin\theta + \cos\theta}. \tag{11}$$

At the cusp point, which is at $(0, 0)$ in the normal form, J_1 has a vertical slope, so W must pass through $(0, 0)$ and have a vertical slope at this point. Hence, using (6), (9), and (11), we must solve the set of equations

$$\begin{cases} \gamma t^2 \cos\theta - t \sin\theta + a &= 0, \\ \gamma t^2 \sin\theta + t \cos\theta + b &= 0, \\ \dfrac{2\gamma t \cos\theta - \sin\theta}{2\gamma t \sin\theta + \cos\theta} &= 0. \end{cases}$$

Note that this equation is not well posed for $\theta = \pm\pi/2$, which is when FC lies at infinity. We find that the fold-cusp bifurcation point is defined as

$$\mathsf{FC} = \mathsf{FC}(\theta,\gamma) := \begin{pmatrix} a \\ b \end{pmatrix} = \left(\frac{\sin^2\theta}{4\gamma\cos\theta}, \frac{-\sin\theta\,(1+\cos^2\theta)}{4\gamma\cos^2\theta} \right)^T. \tag{12}$$

3.2 Cusp-transition bifurcation

The cusp-transition bifurcation curve, denoted C, is given by the values of (a,b) where $W = W_{(z,y)}(\theta,\gamma,a,b)$ passes through the cusp point C_1 at $(0,0)$ in normal-form coordinates. Using (9) this curve can be parameterised as

$$\mathsf{C} = \mathsf{C}(\theta,\gamma) := \left\{ \begin{pmatrix} a \\ b \end{pmatrix} = \begin{pmatrix} -\gamma t^2\,\cos\theta + t\,\sin\theta \\ -\gamma t^2\,\sin\theta - t\,\cos\theta \end{pmatrix} \;\middle|\; t \in \mathbb{R} \right\}. \tag{13}$$

Hence, C is the point-reflection of $W_{(z,y)}(\theta,\gamma,0,0)$ through the origin. Throughout the paper this bifurcation is coloured cyan.

3.3 Inner- and outer-fold bifurcations

At the inner- and outer-fold bifurcations the parabola W is tangent to J_1. Hence, both curves must have equal slopes at an intersection point (z^*,y^*). It is convenient to parameterise J_1 by $s \in \mathbb{R}$ as

$$J_1 := \begin{pmatrix} z \\ y \end{pmatrix} = \begin{pmatrix} 2s^3 \\ -s^2 \end{pmatrix},$$

so that a point on J_1 is determined by the choice of s. Such a point also lies on $W = W_{(z,y)}(\theta,\gamma,a,b)$ if there exists $t = t(s)$ such that (9) gives the same point (z^*,y^*). A tangency occurs if the slope of J_1 at s is the same as the slope of W at $t(s)$. Equating the slopes (6) and (11) gives

$$\begin{aligned} & \frac{dz}{dy} = \frac{2\gamma t(s)\,\cos\theta - \sin\theta}{2\gamma t(s)\,\sin\theta + \cos\theta} = -3s \\ \Leftrightarrow\quad & 2\gamma t(s)\,\cos\theta - \sin\theta = -3s\,[2\gamma t(s)\,\sin\theta + \cos\theta] \\ \Leftrightarrow\quad & t(s) = \frac{\sin\theta - 3s\,\cos\theta}{2\gamma\,(\cos\theta + 3s\,\sin\theta)}. \end{aligned}$$

Hence, a tangency occurs along the curve

$$\mathsf{T} = \mathsf{T}(\theta,\gamma) := \left\{ \begin{pmatrix} a \\ b \end{pmatrix} = \begin{pmatrix} 2s^3 - \gamma t(s)^2\,\cos\theta + t(s)\,\sin\theta \\ -s^2 - \gamma t(s)^2\,\sin\theta - t(s)\,\cos\theta \end{pmatrix} \;\middle|\; s \in \mathbb{R} \right\}. \tag{14}$$

The bifurcation along T can be of inner- or outer-fold type and depends on the second-order derivatives

$$\frac{d^2z}{dy^2} = \frac{2\gamma}{(2\gamma t(s)\,\sin\theta + \cos\theta)^3} =: \kappa_W(s),$$

along W and

$$\frac{d^2z}{dy^2} = \frac{3}{2s} =: \kappa_J(s),$$

along J_1 at the tangency point. For $s > 0$ an inner-fold tangency occurs if $\kappa_W(s) < \kappa_J(s)$ and the tangency is of outer-fold type if $\kappa_W(s) > \kappa_J(s)$. For $s < 0$ the inequalities are precisely the other way around. The tangency switches from inner- to outer-fold type at points on T with $\kappa_W(s) = \kappa_J(s)$, that is, when there is a cubic tangency between W and J_1. The equality $\kappa_W(s) = \kappa_J(s)$ simplifies to

$$2\gamma\,(\cos\theta + 3s\,\sin\theta)^3 = \frac{3}{2s},$$

so that the cubic tangency points are determined by the real values of s that solve

$$27\sin(\theta)^3\,s^4 + 27\cos(\theta)\,\sin(\theta)^2\,s^3 + 9\cos(\theta)^2\,\sin(\theta)\,s^2 + \cos(\theta)^3\,s - \frac{3}{4\gamma} = 0. \tag{15}$$

Roots of this equation correspond to cusp points on T. Since Eq. (15) has degree four in s, we might expect up to four real roots, so that four cusp points could occur on T. In fact, there are at most two real roots, i.e. at most two cusp points on T. We can see this by computing the discriminant of (15) with respect to s and setting it equal to 0:

$$\frac{27^4\sin^8(\theta)\,[64\sin(\theta) + 3\gamma\,\cos^4(\theta)]}{16\gamma^3} = 0.$$

Clearly $\theta = 0$ will always be a solution to this equation, and for any fixed value $\gamma > 0$, there will be a second solution $\theta = \theta_{\mathsf{T}+\mathsf{T}} < 0$ that is the unique solution to $64\sin(\theta) + 3\gamma\,\cos^4(\theta) = 0$. Hence, the θ-axis is divided into three intervals $-\frac{\pi}{2} \le \theta < \theta_{\mathsf{T}+\mathsf{T}}(\gamma)$, $\theta_{\mathsf{T}+\mathsf{T}}(\gamma) < \theta < 0$, and $0 < \theta \le \frac{\pi}{2}$, and in each interval (15) has the same number of real roots.

The actual number of roots is now easily checked. For $0 < \theta < \frac{\pi}{2}$ there are two real roots of (15), say, $s_1(\theta,\gamma) < s_2(\theta,\gamma)$. The tangencies for $-\infty < s < s_1(\theta,\gamma)$ and $s_2(\theta,\gamma) < s < \infty$ are of outer-fold type and the ones for $s_1(\theta,\gamma) < s < s_2(\theta,\gamma)$ are inner-fold bifurcations. At $\theta = 0$, there is only one cusp point on T, because the cusp point associated with root $s_1(0,\gamma)$ lies at infinity. For $\theta_{\mathsf{T}+\mathsf{T}}(\gamma) < \theta < 0$ there are again two cusp points, given by the two real roots $s_2(\theta,\gamma) < s_1(\theta,\gamma)$, so that we now get inner-fold bifurcations for $-\infty < s < s_2(\theta,\gamma)$ and $s_1(\theta,\gamma) < s < \infty$, and outer-fold bifurcations for $s_2(\theta,\gamma) < s < s_1(\theta,\gamma)$. At $\theta = \theta_{\mathsf{T}+\mathsf{T}}(\gamma)$ there is exactly one (degenerate) cusp point on T, because $s_2(\theta_{\mathsf{T}+\mathsf{T}}(\gamma),\gamma) = s_1(\theta_{\mathsf{T}+\mathsf{T}}(\gamma),\gamma)$, and the two cusp points merge. For $-\frac{\pi}{2} < \theta < \theta_{\mathsf{T}+\mathsf{T}}(\gamma)$ there are no cusp points on T and all the tangencies are of inner-fold type. Throughout the paper we colour the inner-fold bifurcation red and the outer-fold bifurcation green.

4 Two-parameter unfolding

The three codimension-one bifurcations derived in Sec. 3 give curves in the (a,b)-parameter plane that separate regions of topologically equivalent global phase portraits. From now on,

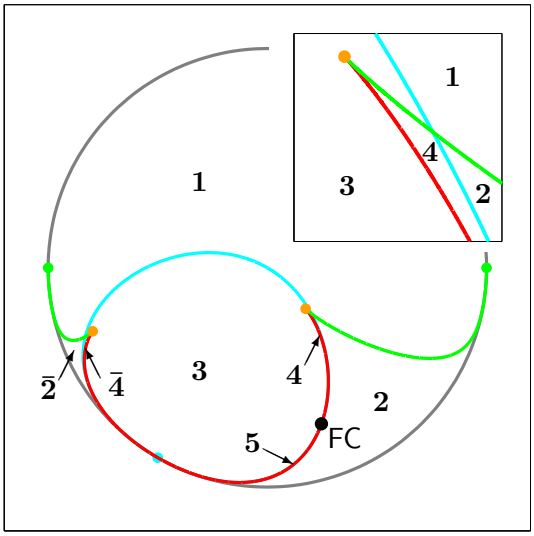

Figure 2: *Two-parameter bifurcation diagram for* $\gamma = 1$ *and* $\theta = \frac{\pi}{3}$ *shown on the Poincaré disk. The colour coding is cyan for the curve of cusp-transition bifurcations, red for inner-fold bifurcations, and green for outer-fold bifurcations. The codimension-two fold-cusp point is marked* FC*. The numbered regions correspond to the topologically different global phase portraits that are illustrated in Fig. 3. A number with a bar on top means that the parabola interacts with* J_1 *as illustrated in the corresponding panels of Fig. 3, but reflected about the* y*-axis.*

we assume $\gamma = 1$ throughout and only classify the different cases with respect to the tilt angle θ. However, as mentioned before, the classification will be entirely equivalent for other values of γ.

As it turns out, the global behaviour of both the phase portraits and the (a, b)-bifurcation diagrams is important for distinguishing the different cases. Therefore, we compactify the (a, b)-parameter plane and the two phase planes in the (z, y)- and (x, y)-coordinates via projection onto the Poincaré disk; this technique is popular in bifurcation theory and was also used in [Krauskopf *et al.*, 2007]. The Poincaré disk is the unit disk in the complex plane. A plane is projected onto this disk via the transformation

$$(u, v) \mapsto \frac{u}{u^2 + v^2 + 1} + \frac{v}{u^2 + v^2 + 1}\, i,$$

so that points $e^{i\phi}$ on the unit circle correspond to the asymptotic directional limits ϕ of curves at infinity.

Figure 2 shows the bifurcation diagram for $\theta = \frac{\pi}{3}$ on the Poincaré disk. The cusp-transition bifurcation (13) is coloured cyan and is the point-reflection about the origin of the parabola $W_{(z,y)}(\frac{\pi}{3}, 1, 0, 0)$. Hence, the angle at infinity is $\theta \pm \pi = -\frac{2\pi}{3}$. The tangency curve (14) has two cusp points where it switches from an outer-fold (green) to an inner-fold (red) bifurcation. On the Poincaré disk the tangency curve always starts at -1 and ends at $+1$. The fold-cusp point is marked FC in the figure. At this point the cusp-transition bifurcation and the inner-fold bifurcation curves are tangent to each other.

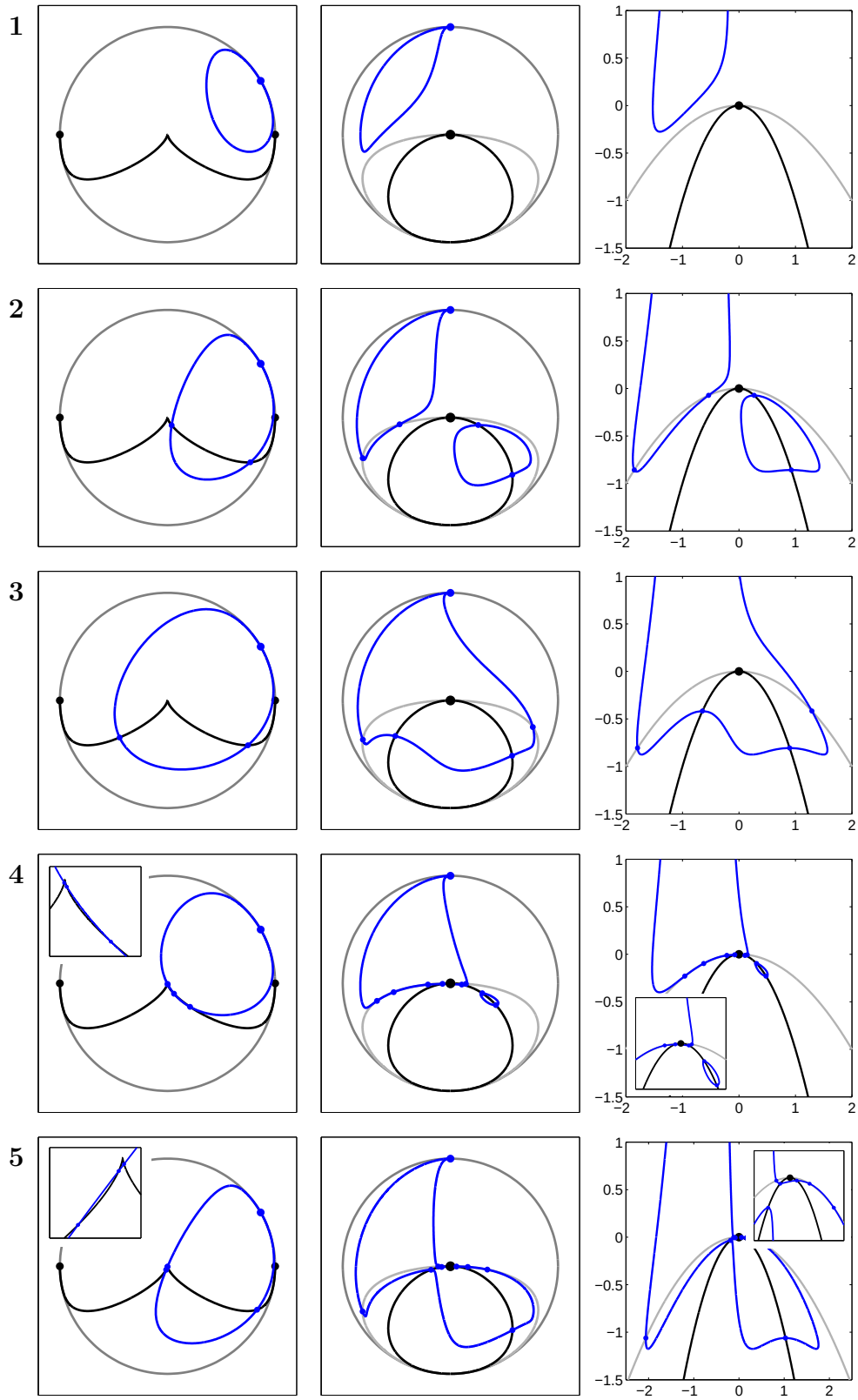

Figure 3: *The first five topologically different global phase portraits of a parabola interacting with J_1 near a cusp point. The left panels show the situation in the (z, y)-plane projected onto the Poincaré disk. The middle and right panels show the effect near J_0 in the (x, y)-plane on the Poincaré disk and in a zoom near the origin, respectively.*

Figure 3 shows representative global phase portraits that correspond to the regions in Fig. 2 bounded by the bifurcation curves. The numbers in Fig. 2 refer to the labels in Fig. 3. There are three pictures associated with each label. The left column in Fig. 3 shows a projection onto the Poincaré disk of a parabola $W_{(z,y)}(\theta,\gamma,a,b)$ (blue) in the (z,y)-plane. The black cusped curve is J_1. The limits of J_1 on the Poincaré disk are -1 and $+1$; for $W_{(z,y)}(\theta,\gamma,a,b)$ they are $e^{i\theta}$ at both ends of the curve. The preimages $W^{-1}_{(x,y)}(\theta,\gamma,a,b)$ of $W_{(z,y)}(\theta,\gamma,a,b)$ are shown in the other two columns of Fig. 3. The middle column shows the projection onto the Poincaré disk and the right column shows a zoom near the origin in the (x,y)-plane. The curves J_0 (black) and $\widehat{J_0}$ (grey) both start and end at the point $e^{-\pi i/2}=-i$ on the Poincaré disk. Note that $W^{-1}_{(x,y)}(\theta,\gamma,a,b)$ always has the limit i, which is true for any $\theta>0$ and $\gamma>0$.

The labels $\bar{2}$ and $\bar{4}$ in Fig. 2 correspond to the regions where the global phase portraits are the mirror images of cases 2 and 4, respectively. For example, as shown in Fig. 3, the parabola in phase portrait 2 intersects J_1 at two points to the right of the cusp point C_1. Hence, the phase portrait associated with $\bar{2}$ will give a parabola with the two intersection points to the left of C_1. Note that, in our terminology, these phase portraits are topologically equivalent.

Figure 3 shows typical phase portraits of how a parabola $W_{(z,y)}(\theta,\gamma,a,b)$ interacts with J_1. For case 1 there are no intersections with J_1 and the preimage $W^{-1}_{(x,y)}(\theta,\gamma,a,b)$ gives another parabola-like curve. Cases 2 and 3 correspond to phase portraits where $W_{(z,y)}(\theta,\gamma,a,b)$ has two intersections with J_1; for case 2 these intersection points lie on the same side of C_1, whereas for case 3 they lie on either side of C_1. The difference between cases 2 and 3 is much more apparent in the respective preimages: $W^{-1}_{(x,y)}(\theta,\gamma,a,b)$ consists of two disjoint branches for case 2, but forms a single curve surrounding the preimage C_0 of C_1 for case 3. A similar difference can be observed between cases 4 and 5. Here $W_{(z,y)}(\theta,\gamma,a,b)$ has four preimages, three on one side for case 4 and two on either side for case 5. For case 4 the preimage $W^{-1}_{(x,y)}(\theta,\gamma,a,b)$ is disjoint: there is one branch surrounding C_0 and another disjoint closed curve further away from C_0. For case 5, on the other hand, $W^{-1}_{(x,y)}(\theta,\gamma,a,b)$ forms a single connected branch that is created as a segment of the parabola-like curve in case 4 passes through the precusp point C_0.

The bifurcation diagram in Fig. 2 and corresponding phase portraits in Fig. 3 are representative for all $0<\theta\leq\frac{\pi}{2}$. At $\theta=\frac{\pi}{2}$ the bifurcation diagram on the Poincaré disk is completely symmetric about the imaginary axis and the fold-cusp point FC lies at $-i$. At $\theta=0$ the cusp-transition curve limits at -1 and there is no left cusp point on the tangency curve. As soon as θ becomes negative, this cusp point reappears on the other side and the limiting end-branches of the tangency curve become inner-fold bifurcations with an outer-fold segment in between the two cusps. This *bifurcation at* ∞ causes a topological change in the bifurcation diagram.

For $-\frac{\pi}{2}\leq\theta<0$ there are four topologically different bifurcation diagrams; see Fig. 4. The transition points $-\frac{\pi}{2}<\theta_{\mathsf{T}+\mathsf{T}}(\gamma)<\theta_{\mathsf{C}+\mathsf{T}}(\gamma)<\theta_{\mathsf{FC}+\mathsf{I}}(\gamma)<0$ are defined as follows.

- At $\theta=\theta_{\mathsf{T}+\mathsf{T}}(\gamma)$ we already know that the two cusp points on T merge and vanish; recall that $\theta_{\mathsf{T}+\mathsf{T}}(\gamma)$ is defined by a non-zero double root $s_1(\theta_{\mathsf{T}+\mathsf{T}}(\gamma),\gamma)=s_2(\theta_{\mathsf{T}+\mathsf{T}}(\gamma),\gamma)$ of Eq. (15).

- At $\theta=\theta_{\mathsf{C}+\mathsf{T}}(\gamma)$ the cusp point defined by root $s_1(\theta_{\mathsf{C}+\mathsf{T}}(\gamma),\gamma)$ lies exactly on the

curve C of cusp-transition bifurcations. This means that $W_{(z,y)}(\theta, \gamma, a, b)$ makes a cubic tangency with J_1, while it also passes through C_1. These two events happen for the same (a, b)-values, but not at the same point (z, y) in the phase plane, so that the bifurcation is of codimension two (the cubic tangency) plus one (the cusp transition), instead of codimension three. We can compute $\theta_{\mathsf{C+T}}$ by equating (13) and (14), where we write $t(s)$ in terms of s and θ, and solving along with Eq. (15).

- At $\theta = \theta_{\mathsf{FC+I}}(\gamma)$ two branches of the inner-fold bifurcation curve pass through FC. That is, $W_{(z,y)}(\theta, \gamma, a, b)$ is tangent to J_1 at C_1 and at the same time tangent to J_1 at another point. Hence, the inner-fold tangencies occur at two different points in phase space, so that the bifurcation is again of codimension two (FC) plus one (inner fold). We can compute $\theta_{\mathsf{FC+I}}$ by equating (12) and (14).

For a given value of γ we can compute these angles by solving the appropriate systems of equations numerically. For $\gamma = 1$ we found $\theta_{\mathsf{T+T}}(\gamma) \approx -0.04669 \approx -\frac{\pi}{67.29}$, $\theta_{\mathsf{C+T}}(\gamma) \approx -0.04473 \approx -\frac{\pi}{70.24}$, and $\theta_{\mathsf{FC+I}}(\gamma) \approx -0.03694 \approx -\frac{\pi}{85.04}$.

Four generic bifurcation diagrams are shown in Fig. 4 to illustrate the topologically different cases. As mentioned, the transition through $\theta = 0$ is a bifurcation at infinity where the role of inner-fold and outer-fold bifurcations is reversed. The representative bifurcation diagram for $\theta = -\frac{\pi}{90}$ is shown in Fig. 4(a). The inner-fold bifurcation curve that passes through FC starts at -1 and ends in the left cusp point. The other inner-fold bifurcation curve starts at the right cusp point close to $+1$, but passes all the way back, close to -1, before practically following the rim of the Poincaré disk to end at $+1$. Figure 4(b) shows the bifurcation diagram for $\theta = -\frac{\pi}{75}$. The situation is very similar to Fig. 4(a), except that the inner-fold bifurcation curve that does not pass through FC now cuts across the Poincaré disk above FC instead of below FC as in Fig. 4(a). Figure 4(c) shows the bifurcation diagram for $\theta = -\frac{\pi}{69}$, where both cusp points on the tangency curve T lie on the same side of the cusp-transition curve C. Finally, for any $-\frac{\pi}{2} < \theta < \theta_{\mathsf{T+T}}$ the bifurcation diagram is equivalent to Fig. 4(d), which shows the bifurcation diagram for $\theta = -\frac{\pi}{6}$. Note that the bifurcation diagram for $\theta = -\frac{\pi}{2}$ is completely symmetric about the imaginary axis, as was the case for $\theta = \frac{\pi}{2}$, but FC now lies at $+i$.

The bifurcation diagrams in Fig. 4 give rise to a further eight different global phase portraits, shown in Figs. 5 and 6. Observe that for $\theta < 0$ the parabola-like preimages of $W_{(z,y)}(\theta, \gamma, a, b)$ always end at $-i$ on the Poincaré disk (middle column of the figures). Since $\theta_{\mathsf{T+T}} \approx -\frac{\pi}{67.29}$, most negative angles θ lead to a bifurcation diagram equivalent to Fig. 4(d) with only the topologically different global phase portraits 6 (equivalent to $\bar{6}$), 8, 11, and 12. As shown in Figs. 5 and 6, these phase portraits all show cases where $W_{(z,y)}(\theta, \gamma, a, b)$ intersects J_1 at most four times, just as for $0 < \theta \leq \frac{\pi}{2}$. Recall from (10) that we should also expect cases with six intersections between $W_{(z,y)}(\theta, \gamma, a, b)$ and J_1. For $\gamma = 1$ this only occurs for negative θ-values very close to 0, and leads to cases 9 and 10.

5 Local bifurcation diagram near FC

The bifurcation diagrams in Figs. 2 and 4 show that the fold-cusp bifurcation point FC is always formed by a tangency between the curve C of cusp-transition bifurcations and a curve

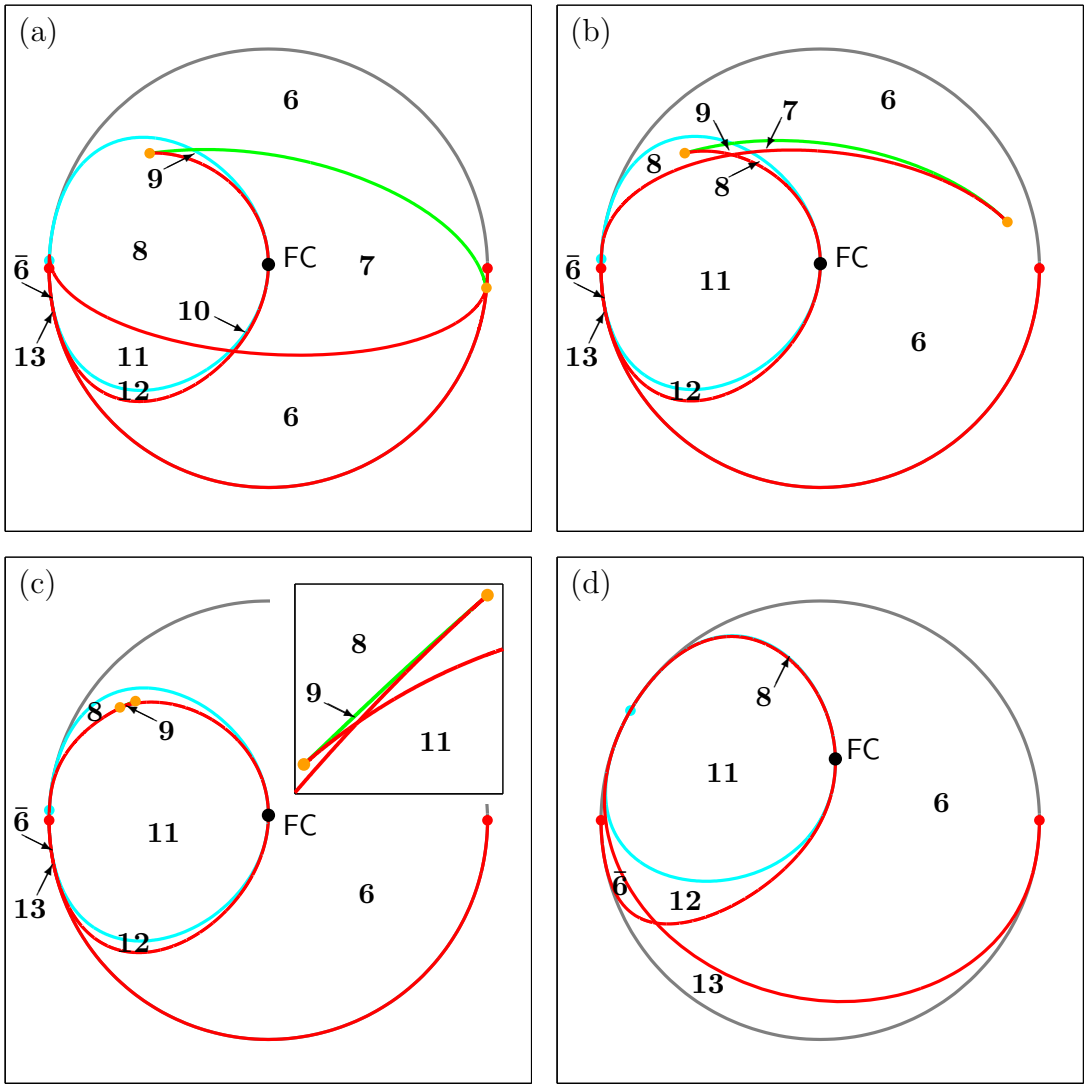

Figure 4: *Two-parameter bifurcation diagrams for $\gamma = 1$ and $\theta < 0$; shown are the four topologically different cases in projection onto the Poincaré disk, represented by $\theta = -\frac{\pi}{90}$, $\theta = -\frac{\pi}{75}$, $\theta = -\frac{\pi}{69}$, and $\theta = -\frac{\pi}{6}$, respectively. The colour coding is as in Fig. 2 and the numbered regions correspond to the topologically different global phase portraits that are illustrated in Figs. 5 and 6.*

I of inner-fold bifurcations. Indeed, it is not hard to show that the tangency of a parabola with J_1 at the cusp point C_1 must be of inner-fold type. In order to visualise the position of I relative to C, we plot the two curves in Fig. 7 with the distance in a from C as the horizontal axis. Figure 7(a) shows the local bifurcation diagram for $\theta = \frac{\pi}{3}$ with the labels in each region indicating the associated topologically equivalent phase portraits as given in Fig. 3; compare also Fig. 2. Similarly Figs. 7(b) and (c) show the local bifurcation diagrams for $\theta = -\frac{\pi}{90}$ and $\theta = -\frac{\pi}{6}$, respectively; compare Figs. 4(a) and (d). The labels in each region again indicate the associated topologically equivalent phase portraits as given in Figs. 5 and 6. Note that Fig. 7(c) is representative for all $-\frac{\pi}{2} < \theta < \theta_{\mathsf{FC+I}}(\gamma)$; see Figs. 4(b) and (c).

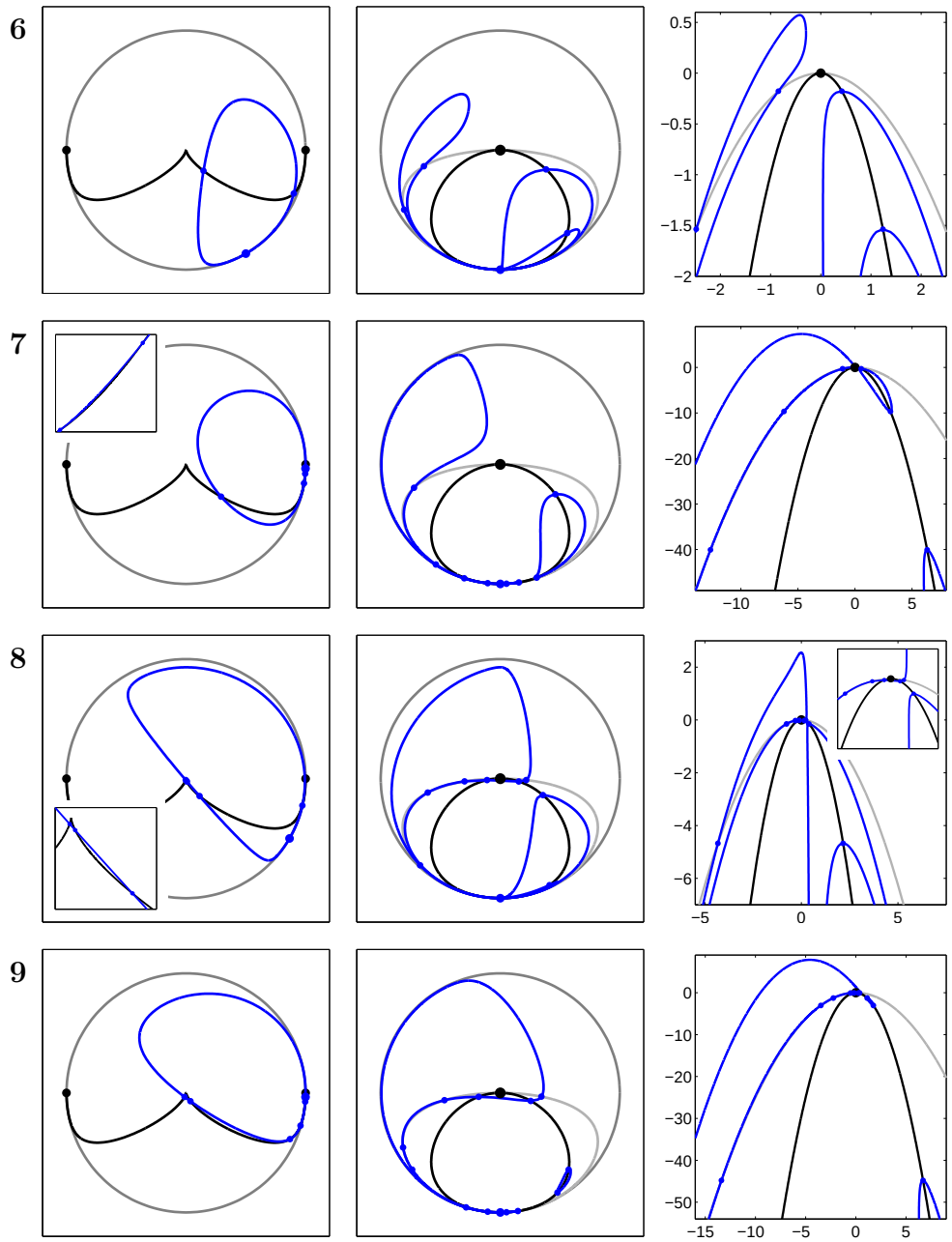

Figure 5: *Four of the thirteen topologically different global phase portraits of a parabola interacting with J_1 near a cusp point. The left panels show the situation in the (z, y)-plane projected onto the Poincaré disk. The middle and right panels show the effect near J_0 in the (x, y)-plane on the Poincaré disk and in a zoom near the origin, respectively; see also Figs. 3 and 6.*

Figure 7 shows that the curve I of inner-fold bifurcations makes a cubic tangency with the curve C of cusp-transition bifurcations. Indeed, for arbitrary $-\frac{\pi}{2} < \theta < \frac{\pi}{2}$ and $\gamma > 0$ both derivatives $\frac{da}{db}$ and $\frac{d^2a}{db^2}$ are the same along C and I at the codimension-two point FC.

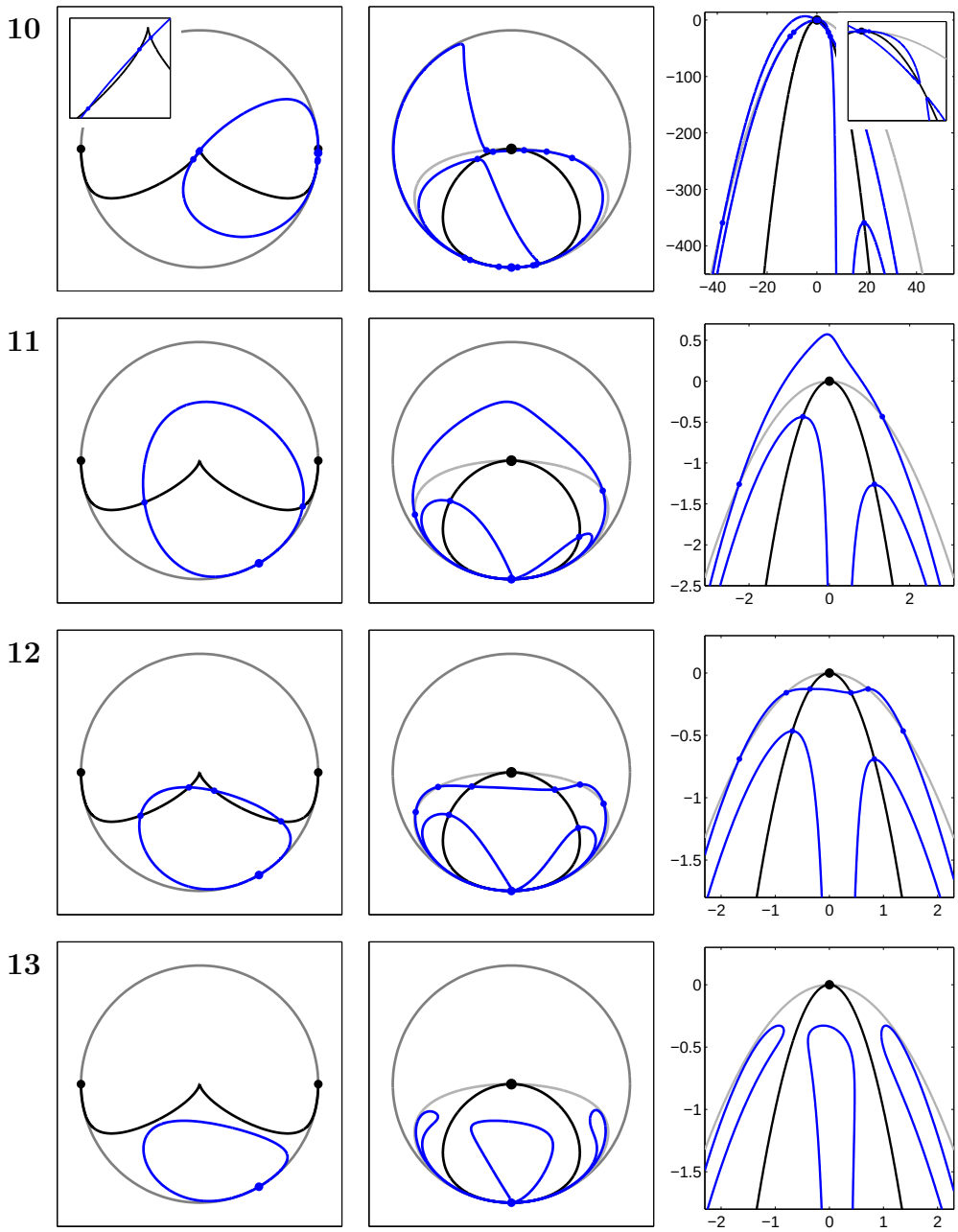

Figure 6: *Four of the thirteen topologically different global phase portraits of a parabola interacting with J_1 near a cusp point. The left panels show the situation in the (z, y)-plane projected onto the Poincaré disk. The middle and right panels show the effect near J_0 in the (x, y)-plane on the Poincaré disk and in a zoom near the origin, respectively; see also Figs. 3 and 5.*

We conclude that there is only one local bifurcation diagram near the fold-cusp bifurcation, but the associated global phase portraits give rise to three different cases. Indeed, the global phase portraits 2, 5, 3, and 4 in Fig. 7(a) are topologically different from the respective global phase portraits 7, 10, 8, and 9 in Fig. 7(b) and 6, 12, 11, and 8 in Fig. 7(c), because

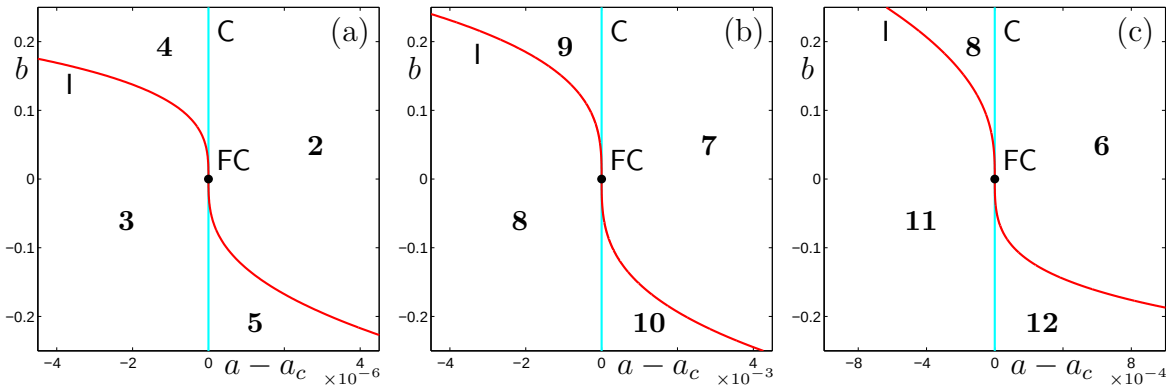

Figure 7: *Local unfolding of the fold-cusp bifurcation point* FC *showing the relative position of the inner-fold curve* I *with respect to the cusp-transition curve* C*. The horizontal axis is the distance in the parameter* a *from* C*, which appears as the cyan vertical axis; the different regions give rise to phase portraits that are topologically equivalent to the phase portraits corresponding to the labels as given in Figs. 3, 5, and 6. The parameters are* $\gamma = 1$ *and* θ *is* $\frac{\pi}{3}$ *in panel (a),* $-\frac{\pi}{90}$ *in panel (b), and* $-\frac{\pi}{6}$ *in panel (c).*

the angle θ does not have the same sign; see Figs. 3, 5, and 6. Furthermore, phase portraits 9 and 10 in Fig. 7(b) are the only two global phase portraits that involve six intersections with J_1, so that this case is different from that in Fig. 7(c). Hence, there are four topologically different global phase portraits near the fold-cusp point FC, but which four depends on the value of θ.

Let us take a closer look at the phase portraits locally near FC for the cases shown in Figs. 7(a) and 7(b), i.e., compare phase portraits 2 with 7, 3 with 8, 4 with 9, and 5 with 10 in Figs. 3, 5, and 6. In fact, *locally* near the cusp point C_1, these phase portraits are pairwise topologically equivalent. Indeed, for each pair of corresponding phase portraits in Figs. 7(a) and 7(b) we can choose a local segment, that is, a finite part of the parabola without the two branches that go off to infinity, so that the phase portaits are topologically identical. To be more precise, Definition 2.1 has a local equivalent that says the following.

Definition 5.1 (Local topological equivalence with respect to J_1) *Two curves are locally topologically equivalent if for each curve we can restrict to a finite segment, such that the following holds:*

1. *The four end points of the segments lie either all in the region Z_1 above J_1, or all in the region Z_3 below J_1.*

2. *The number of intersection points of the segments with J_1 is the same.*

3. *The order in which these intersection points lie on J_1 relative to the cusp point C_1 is the same.*

For example, we can take a finite segment of $W_{(z,y)}(\theta, \gamma, a, b)$ in phase portrait 2 of Fig. 3 that has both end points in the region Z_1 above J_1 with a short segment passing through Z_3

below J_1, which creates the two intersections with J_1. The parabola in phase portrait 7 of Fig. 5 has four intersections with J_1, but we can select a finite segment that starts in between the first and second intersections and ends in between the third and fourth intersections. Then this segment also has both end points in Z_1 with a short segment passing through Z_3. In other words, phase portraits 2 and 7 are two *global manifestations of the same local phase portrait*.

Clearly, any parabola $W_{(z,y)}(\theta, \gamma, a, b)$ with $\gamma > 0$, $\theta_{\mathsf{FC+I}}(\gamma) < \theta < 0$, and a and b such that its global phase portrait is topologically equivalent to case 7 of Fig. 5 is locally topologically equivalent to the local phase portrait of case 2 of Fig. 3. Similarly, the phase portraits of cases 3 and 8 are locally topologically equivalent, as are the pairs 4 and 9, and 5 and 10.

The phase portraits for cases 6, 11, 8 and 12 in Fig. 7(c), however, are not locally topologically equivalent to the corresponding phase portraits of Figs. 7(a) or (b). For example, any finite segment of the parabola in phase portrait 6 of Fig. 5 that intersects J_1 twice will have both end points in Z_3 and not in Z_1 as required for local topological equivalence with phase portraits 2 or 7. Hence, at the level of local topological equivalence there are only two different cases for the local unfolding of the codimension-two fold-cusp bifurcation; these two cases are for $-\frac{\pi}{2} \leq \theta < \theta_{\mathsf{FC+I}}(\gamma)$ and $\theta_{\mathsf{FC+I}}(\gamma) < \theta < \frac{\pi}{2}$, given by Figs. 7(c) and (a), respectively, together with the associated local phase portraits as indicated by the labels.

In summary, we find that, generically, we expect to see phase portraits that are locally topologically equivalent to cases 2, 3, 4, or 5 in Fig. 3 or 6, 8, 11, or 12 in Figs. 5 and 6 with a two-parameter bifurcation diagram that is topologically equivalent to Figs. 7(a) or (c). Only outside a neighbourhood of FC is it possible to obtain phase portaits that are locally topologically equivalent to cases 1 in Fig. 3 or 13 in Fig. 6.

In an even smaller neighbourhood of C_1 phase portraits 6 and 2 could be considered locally topologically equivalent if we allow that the two finite segments in Definition 5.1 can be chosen such that each has one end point in Z_1 and the other in Z_3. Effectively, this amounts to the three-parameter analysis (with $\gamma = 0$) of the interaction of a straight line with J_1 in the neighbourhood of the cusp point C_1. A straight line can only be tangent to J_1 at C_1 if it is vertical, so that variation of θ must always be present in order to obtain all topologically different cases. Note that a and b then play essentially the same role, so that there is only one single two-parameter bifurcation diagram for the fold-cusp bifurcation. Furthermore, the phase portraits for a straight line that correspond to local phase portraits of, say, 6 and 11 in Fig. 7(c) are topologically equivalent up to symmetry. Similarly, 8 and 12 in Fig. 7(c) are related by symmetry, as are the corresponding pairs of phase portraits in Fig. 7(a). On the other hand, a backward invariant curve is typically not straight, not even in a neighbourhood of the cusp point C_1, so that we can still expect to distinguish the two topologically different cases given by $-\frac{\pi}{2} \leq \theta < \theta_{\mathsf{FC+I}}$ and $\theta_{\mathsf{FC+I}} < \theta \leq \frac{\pi}{2}$ at the level of local topological equivalence for a quadratic curve, albeit in a possibly very small neighbourhood of FC in the (a, b)-plane.

6 Conclusion

We considered the unfolding of the fold-cusp bifurcation, defined as the moment when a segment W of a backward invariant set is tangent to the critical locus J_1 at a cusp point C_1.

In our analysis, we assumed that locally we may approximate W by a parabola that is defined in local coordinates, where C_1 is the origin, by a quadratic coefficient γ, a tilt angle θ and a translation (a, b); we consider γ and θ as higher-order parameters and only vary the two parameters a and b. Under the assumption that W is globally a parabolic curve, we find that the fold-cusp bifurcation gives rise to five topologically different two-parameter bifurcation diagrams, associated with a total of thirteen topologically different global phase portraits. For any fixed $\gamma \neq 0$ all five bifurcation diagrams can be obtained by varying θ; similarly, one can also fix θ and vary γ, as long as $\theta \notin \{-\frac{\pi}{2}, 0, \frac{\pi}{2}\}$. Locally in a neighbourhood of the fold-cusp bifurcation point FC, only two codimension-one bifurcations can occur, namely, the cusp-transition bifurcation C and the inner-fold bifurcation I. At the codimension-two point FC the curves C and I have a cubic tangency, separating the parameter space locally into four different regions. At this local level, there are two topologically different cases if we only consider local topological equivalence of the phase portraits.

Generically, if a curve W passes through a neighbourhood of the cusp point C_1 then it either intersects J_1 two or four times locally in this neighbourhood; the four regions of local topological equivalence in each of the local bifurcation diagrams distinguish the order and number of intersections on either side of C_1. In particular, it is not possible to choose parameter values in a sufficiently small neighbourhood of FC such that W does not intersect J_1 at all.

The bifurcation curves in the (a, b)-parameter space that are shown in Figs. 2 and 4 can be thought of as slices of bifurcation surfaces in the three-dimensional (θ, a, b)-space. These particular bifurcation surfaces are familiar objects from singularity theory; they arise, for example, as the bifurcation set of the boundary singularity B_3 [Arnol′d, 1978]. This illustrates one of the key concepts of singularity theory, namely, that certain situations are generic and one expects to see them in many different contexts. For the analysis in this paper we utilized not only this genericity concept, but also classical techniques from singularity theory, such as the computation of discriminants, in order to locate repeated roots, and higher-order derivatives, in order to distinguish between different cases. From the point of view of singularity theory, it may be interesting to see if the study of functions from the plane to the plane that keep J_1 fixed also generate the five topologically different two-parameter bifurcation diagrams; see, for example, [Bruce, 1984, Bruce & West, 1998]. From the point of view of dynamical systems theory, however, we are primarily interested in using bifurcation theory to characterise the interaction of the stable set with the critical locus. This approach is popular in the standard context of smooth vector fields and diffeomorphisms; see, for example, [Guckenheimer & Holmes, 1983, Kuznetsov, 2004]. They are also powerful when used, for example, for systems with symmetry [Golubitsky & Shaeffer, 1985, Golubitsky *et al.*, 1988]. Our work is very much in the spirit of the papers [England *et al.*, 2005, Krauskopf *et al.*, 2007] on planar endomorphisms, but it is also close in spirit to bifurcation theory in other contexts. For example, piecewise-smooth systems are characterised by a critical locus where the flow or map changes in a non-smooth or discontinuous way. The study of periodic orbits of a piecewise-smooth system interacting with such a critical locus is very similar to what we have done here; see [Kuznetsov *et al.*, 2003, Kowalczyk *et al.*, 2006]. Furthermore, the study of how the geometry is organised by such discontinuities has a similar flavour [Chillingworth, 2002]. We also point to recent work on the dynamics of return maps on a global Poincaré section, where

the first-return map is typically not continuous [Judd *et al.*, 2007].

Acknowledgements

We thank Bernd Krauskopf for many helpful conversations during the writing of this paper. CAH thanks the Department of Mathematics, University of Bristol, for its hospitality while this research was conducted. The research of HMO was supported by an Advanced Research Fellowship grant of the Engineering and Physical Sciences Research Council (EPSRC).

References

Adomaitis, R.A. & Kevrekidis, I.G. [1991] "Noninvertibility and structure of basins of attraction in a model adaptive control system," *J. Nonlin. Sci.* **1**(1): 95–105.

Agliari, A. [2000] "Global bifurcations in the basins of attraction in noninvertible maps and economic applications," *Nonlin. Anal.* **47**(8): 5241–5252.

Agliari, A., Gardini, L. & Mira, C. [2003] "On the fractal structure of basin boundaries in two-dimensional noninvertible maps," *Int. J. Bifurcation & Chaos* **13**(7): 1767–1785.

Arnol′d, V.I. [1978] "Critical points of functions on the manifold with boundary, simple Lie groups B_k, C_k, F_4 and singularities of evolutes," *Russian Math. Surveys* **33**(5): 91–105.

Back, A., Guckenheimer, J., Myers, M.R., Wicklin, F.J. & Worfolk, P.A. [1992] "DsTool: Computer assisted exploration of dynamical systems," *Notices Amer. Math. Soc.* **39**: 303–309.

Bischi, G.-I., Gardini, L. & Mira, C. [2006] "Basin fractalizations generated by a two-dimensional family of $(Z_1 - Z_3 - Z_1)$ maps," *Int. J. Bifurcation & Chaos* **16**(3): 647–669.

Bruce, J.W. [1984] "Functions on discriminants," *J. London Math. Soc.* **30**(2): 551–567.

Bruce J.W. & West J.M. [1998] "Functions on cross-caps," *Math. Proc. Camb. Phil. Soc.* **123**: 19–39.

Chillingworth, D.R.J. [2002] "Discontinuity geometry for an impact oscillator," *Dyn. Sys.* **17**(4): 389–420.

Cox, D., Little, J. & O'Shea, D. [1997] *Ideals, Varieties, and Algorithms: An Introduction to Computational Algebraic Geometry and Commutative Algebra*, Undergraduate texts in mathematics, Springer-Verlag, New York, second edition.

England, J.P., Krauskopf, B. & Osinga, H.M. [2004] "Computing one-dimensional stable manifolds of planar maps without the inverse," *SIAM J. Appl. Dyn. Syst.* **3**(2): 161–190.

England, J.P., Krauskopf, B. & Osinga, H.M. [2005] "Bifurcations of stable sets in noninvertible planar maps," *Int. J. Bifurcation & Chaos* **15**(3): 891–904.

Frouzakis, C.E., Adomaitis, R.A., Kevrekidis, I.G., Golden, M.P. & Ydstie, B.E. [1992] "The structure of basin boundaries in a simple adaptive control system," in *Chaotic Dynamics: Theory and Practice*, T. Bountis (ed.), Plenum Press, New York, pp. 195–210.

Frouzakis, C.E., Gardini, L., Kevrekidis, I.G., Millerioux, G., & Mira, C. [1997] "On some properties of invariant sets of two-dimensional noninvertible maps," *Int. J. Bifurcation & Chaos* **7**(6): 1167–1194.

Golubitsky, M. & Schaeffer, D.G. [1985] *Singularities and Groups in Bifurcation Theory: Vol. I*, Applied Mathematical Sciences **51**, Springer-Verlag, New York.

Golubitsky, M., Stewart, I.N. & Schaeffer, D.G. [1988] *Singularities and Groups in Bifurcation Theory: Vol. II.*, Applied Mathematical Sciences **69**, Springer-Verlag, New York.

Guckenheimer, J. & Holmes, P. [1983] *Nonlinear Oscillations, Dynamical Systems, and Bifurcations of Vector Fields*, Springer-Verlag, New York, second printing.

Josić, K. & Sander, E. [2004] "The structure of synchronization sets for noninvertible systems," *Chaos* **14**(2): 249–262.

Judd, C., Krauskopf, B. & Osinga, H.M. [2007] "Tangency bifurcations of global Poincaré maps," Bristol Centre for Applied Nonlinear Mathematics Preprint BCANM.950, 2007.

Krauskopf, B., Osinga, H.M. & Peckham, B.B. [2007] "Unfolding the cusp-cusp bifurcation of planar endomorphisms," *SIAM J. Appl. Dyn. Sys.* **6**(2): 403–440.

Kowalczyk, P., di Bernardo, M., Champneys, A.R., Hogan, S.J., Homer, M., Piiroinen, P.T., Kuznetsov, Yu.A. & Nordmark, A. [2006] "Two-parameter discontinuity-induced bifurcations of limit cycles: classification and open problems," *Int. J. Bifurcation & Chaos* **16**(3): 601–629.

Kuznetsov, Yu.A. [2004] *Elements of Applied Bifurcation Theory*, Springer-Verlag, New York/Berlin, third edition.

Kuznetsov, Yu.A., Rinaldi, S. & Gragnani, A. [2003] "One-parameter bifurcations in planar Filippov systems," *Int. J. Bifurcation & Chaos* **13**(8): 2157–2188.

López-Ruiz, R. & Fournier-Prunaret, D. [2003] "Complex patterns on the plane: different types of basin fractalization in a two-dimensional mapping," *Int. J. Bifurcation & Chaos* **13**(2): 287–310.

Mira, C. & Shilnikov, A. [2005] "Slow-fast dynamics generated by noninvertible plane maps," *Int. J. Bifurcation & Chaos* **15**(11): 3509–3534.

Palis, J. & de Melo, W. [1982] *Geometric Theory of Dynamical Systems*, Springer-Verlag, New York.

Ugarcovici, I. & Weiss, H. [2004] "Chaotic dynamics of a nonlinear density dependent population model," *Nonlinearity* **17**(5): 1689–1711.

Wikan, A. & Mjølhus, E. [1996] "Overcompensatory recruitment and generation delay in discrete age-structured population models," *J. Math. Biol.* **35**(2): 195–239.